

## 180 Wrapped Tubes

Herbert Edelsbrunner

Department of Computer Science, Duke University, Durham, NC 27708  
and Raindrop Geomagic, Research Triangle Park, NC 27709.

**Abstract:** The 180 models collected in this paper are produced by sampling and wrapping point sets on tubes. The surfaces are represented as triangulated 2-manifolds and available as `stl`-files from the author's web site at `www.cs.duke.edu/~edels`. Each tube is obtained by thickening a circle or a smooth torus knot, and for some we use the degrees of freedom in the thickening process to encode meaningful information, such as curvature or torsion.

**Keywords:** Surface reconstruction, geometric design, differential geometry.

**Categories:** G.2.m.

### 1 Tubes

This paper provides a visual index into a collection of 180 tubes. In other words, there are three tubes for each year of Hermann's current age. That ratio will go down and we expect it to approach zero. Each tube is defined by a simple planar figure sweeping along to a curve in space. The curve is the image of a smooth map  $\Gamma : \mathbb{R} \rightarrow \mathbb{R}^3$ . To perform a sweep, we move the Frenet frame along the curve. This is the orthonormal coordinate system spanned by the unit tangent, normal, and binormal vectors. The tangent vector is the normalized first derivative. The normal vector lies in the osculating plane spanned by the first two derivatives. The binormal is the cross-product of the tangent and the normal vectors. It is convenient to change the order and compute the normal as the cross-product of the tangent and the binormal vectors:

$$\begin{aligned}T(s) &= \dot{\Gamma}(s) / \|\dot{\Gamma}(s)\|, \\N(s) &= B(s) \times T(s), \\B(s) &= \dot{\Gamma}(s) \times \ddot{\Gamma}(s) / \|\dot{\Gamma}(s) \times \ddot{\Gamma}(s)\|.\end{aligned}$$

$T$ ,  $N$ ,  $B$  vary smoothly with the parameter provided there is no  $s$  for which  $\dot{\Gamma}(s)$  and  $\ddot{\Gamma}(s)$  are linearly dependent. Refer to standard texts in differential geometry for general background on smooth curves [1, 2].

The models depicted in Figures 1 through 15 are obtained by computing sample points on the tubes and reconstructing the surface with the Wrap software of Raindrop Geomagic [4]. Boundary and feature lines are sampled with higher frequency to aid the reconstruction. The local regularity of the produced surface triangulations is a side-effect of the regular point sampling. Close inspection reveals local irregularities where

triangulations adopt to the local curvature and to non-regular point distributions. All surfaces are watertight triangulations that can be used to manufacture the models with layered technology 3D printers.

## 2 Tori

All tori in Figures 1 through 5 are generated by sweeping a planar figure along a circle in space. Assuming this circle has radius  $R$  and lies in the  $xy$ -plane symmetric around the origin we have

$$\Gamma(s) = \begin{pmatrix} R \cos s \\ R \sin s \\ 0 \end{pmatrix}.$$

The vectors  $T$ ,  $N$ ,  $B$  spanning the Frenet frame are readily computed from  $\Gamma$ ,  $\dot{\Gamma}$ ,  $\ddot{\Gamma}$ . Different tori are distinguished by the form of the planar figure and the number of times it rotates relative to its frame. We have line segments, triangles, squares, pentagons, and hexagons as cross-sections.

**Line segment.** The models are shown in Figure 1. Each model is a surface with boundary and does not bound any volume. The surface is orientable if and only if the number of rotations is integer. The first model in the first row of Figure 1 is a Möbius strip obtained by sweeping with a half rotation.

**Triangle.** The models are shown in Figure 2. With increasing number of rotations, the dihedral angles get sharper and pose a progressively more severe challenge to the reconstruction method.

**Square.** The models are shown in Figure 3. To count rotations, we count the corners in the projection of the hole through the middle. To determine the sign, we see whether the tube curls towards the middle in a clockwise or in a counter-clockwise direction.

**Pentagon.** The models are shown in Figure 4. The negative rotation produces shapes that can also be obtained by positive rotation followed by reflection through a plane. In  $\mathbb{R}^3$ , negative and positive rotation generate two different families of shapes with opposite sense.

**Hexagon.** The models are shown in Figure 5. The projection of the middle hole changes from convex to non-convex as the number of rotations exceeds six. Similarly for the line segment, triangle, square, and pentagon, the transition from convex to non-convex happens when the number of rotations reaches the number of sides.

## 3 Knots

All knots in Figures 6 through 11 are generated by sweeping a fixed planar figure along strands that wind around a torus. Strictly speaking, we have links and not just knots

because the strands may close up to form more than one closed curve. Let  $R$  be the radius of the center circle and  $r$  the radius of the meridian circle. Assuming the center circle lies in the  $xy$ -plane symmetric around the origin, the torus consists of points

$$\begin{pmatrix} R \cos s - r \sin t \cos s \\ R \sin s - r \sin t \sin s \\ r \cos t \end{pmatrix},$$

for  $s, t \in [0, 2\pi)$ . We get a closed curve by setting  $t = \omega \cdot s$  for some rational  $\omega$ . As  $T$  traverses once around the length of the torus, it winds  $\omega$  times around the meridian. It closes up after traversing the length  $k$  times around, where  $k \cdot \omega$  is the smallest integer multiple of  $\omega$ .

Consider for example the third model in the first row of Figure 11. This is the trefoil knot obtained by setting  $\omega = \frac{3}{2}$  and following the torus around twice. Alternatively, the trefoil knot is obtained from two strands each traversing the length of the torus once while winding  $\frac{3}{2}$  times around the meridian. The two strands are diagonally opposite on the meridian circles and meet to form the connected center curve of the knot. That center curve is traced out by the endpoints of a line segment that sweeps along the center circle and rotates  $\frac{3}{2}$  times in one round. The surface swept out by the line segment is the non-orientable strip shown in position three in the first row of Figure 1. Different knots are distinguished by

- (1) the form of the planar figure,
- (2) the number of parallel strands,  $\lambda$ ,
- (3) the number of times a strand winds around the meridian,  $\omega$ ,
- (4) the number of times the cross-section rotates relative to its frame,  $\varrho$ .

We have line segments, triangles, squares, pentagons, hexagons, and circles as cross-sections. Numbers  $\omega$  and  $\varrho$  are counted once around the length of the torus. Triplets  $(\lambda, \omega, \varrho)$  are used as names for the knots, assuming the figure of the cross-section is understood. In the case of a circle,  $\varrho$  is irrelevant and dropped from the name. For example we have a trefoil knot whenever  $\lambda = 2, \omega = \frac{3}{2}$  or  $\lambda = 3, \omega = \frac{2}{3}$ . We find versions of the trefoil knot in Figures 6, 9, 11, 13, 14.

**Line segment.** The models are shown in Figure 6. The twisting of a strip is a combination of the turning of the Frenet frame and the rotation of the line segment relative to that frame. Since the frame returns to its initial position, orientability depends merely on the number of rotations: the strip is orientable if and only if  $\varrho$  is integer.

**Triangle.** The models are shown in Figure 7. The torsion is the amount of turning or sideways rolling of the frame as it sweeps along the curve. If  $\varrho = 0$ , this is directly visible from how much the cross-section twists.

**Square.** The models are shown in Figure 8. The models in the first row differ from the others by sweeping the square in diamond position within the Frenet frame. The

number of components is the greatest common divisor of  $\lambda$  and  $\lambda \cdot \omega$ . The models in Figure 8 consisting of two components are  $(2, \frac{6}{2}, 0)$ ,  $(2, \frac{8}{2}, 0)$ , and  $(4, \frac{2}{4}, 0)$ .

**Pentagon.** The models are shown in Figure 9. All torus knots with  $\lambda = 1$  or  $\lambda \cdot \omega \in \{-1, 0, 1\}$  are trivial: they can be continuously deformed into a standard torus without committing self-intersections in the process. All other torus knots are non-trivial.

**Hexagon.** The models are shown in Figure 10. The speed of the curve is the length of the first derivative. For non-zero  $\varrho$ , the amount of rotation is proportional to the speed. It can be observed from the difference between the twisting for  $\varrho$  and for 0 rotation. We have  $\omega = 1$  for the models in the first and in the last row. If  $R = 2r$ , then the motion of the Frenet frame has a discontinuity at  $\cos t = 0$  and  $\sin t = 1$ . This is the reason for the rapid twisting in the neighborhood of the point where the curve passes through the narrow neck of the torus.

**Circle.** The models are shown in Figure 11. Three of the twelve knots consist of  $\gcd(\lambda, \lambda \cdot \omega) > 1$  components. Six of the remaining nine models are non-trivial knots: the 3rd and 7th are equivalent and known as the trefoil knot, the 4th is Solomon's seal knot, and the 8th, 9th, 12th are usually referred to as torus knots  $T_{3,4}$ ,  $T_{3,5}$ ,  $T_{4,11}$ , see [3, 5].

#### 4 Hoses

We use the freedom to deform the shape of the planar figure during the sweep to visualize the norm  $\nu(s)$ , the speed  $\sigma(s)$ , the curvature  $\kappa(s)$ , and the torsion  $\tau(s)$ . The norm is the distance from the origin and depends on the placement in space, the speed is a function of the parametrization, and the curvature and torsion relate to the shape of the curve. Formulas that work for general and not necessarily unit-speed parametrizations can be found in [2]:

$$\begin{aligned}\nu(s) &= \|\Gamma(s)\|, \\ \sigma(s) &= \|\dot{\Gamma}(s)\|, \\ \kappa(s) &= \|\dot{\Gamma}(s) \times \ddot{\Gamma}(s)\| / \|\dot{\Gamma}(s)\|^3, \\ \tau(s) &= \langle \dot{\Gamma}(s) \times \ddot{\Gamma}(s), \dot{\ddot{\Gamma}}(s) \rangle / \|\dot{\Gamma}(s) \times \ddot{\Gamma}(s)\|^2.\end{aligned}$$

The curvature  $\kappa(s)$  is one over the radius of the osculating circle in the osculating plane at  $\Gamma(s)$ . It thus measures the forward or backward rolling motion of the Frenet frame. The torsion  $\tau(s)$  measures the sideways rolling motion of the frame. The sign of  $\tau(s)$  distinguishes rolling to the left from rolling to the right.

**Norm.** The models are shown in Figure 12. The cross-section is a circle with radius proportional to the norm,  $\nu(s)$ . The tubes appear to adjust their local size to the amount of available space.

**Speed.** The models are shown in Figure 13. For given  $s$  and  $t = \omega \cdot s$ , the speed is

$$\sigma(s) = \sqrt{R^2 + \omega^2 r^2 - 2Rr \sin t + r^2 \sin^2 t}.$$

It assumes its minimum,  $\sigma(s) = R - r$ , whenever  $\omega = 0$  and  $\sin t = 1$ . We transform speed using  $f(x) = \frac{R-r}{x}$  and produce the models by sweeping a circular cross-section with radius proportional to  $f \circ \sigma(s)$ . Growing  $\omega$  increases speed and produces progressively skinnier tubes that wind more and more around the meridian.

**Curvature.** The models are shown in Figure 14. Assuming  $r < R - r$ , the interval from minimum to supremum curvature is  $[0, \frac{1}{r})$ . We map this interval to  $[1, \infty)$  using  $f(x) = \frac{1}{1-rx}$ . The cross-section of the tube is an ellipse of constant area whose aspect ratio is  $f \circ \kappa(s)$ . The ellipse does not rotate within its frame and the major axis is aligned with the binormal vector,  $B(s)$ .

**Torsion.** The models are shown in Figure 15. Of the four properties considered in this section, torsion is perhaps most difficult to observe directly. It has a sign, which distinguishes rolling to the left from rolling to the right. We only visualize the unsigned quantity, which we transform using  $f(x) = 1 + R \cdot |x|$ . The cross-section is an area preserving ellipse with aspect ratio  $f \circ \tau(s)$ . The ellipse does not rotate within its frame and the major axis is aligned with the normal vector,  $N(s)$ . Note that for small but not too small  $\omega$ , the torsion gets rather large when  $\Gamma$  passes through the narrow neck of the torus. This is reflected by a skinny ellipse generating a pronounced ridge on the tube.

## References

1. J. W. BRUCE AND P. J. GIBLIN. *Curves and Singularities*. Cambridge Univ. Press, Cambridge, England, 2nd edition, 1992.
2. A. GRAY. *Modern Differential Geometry of Curves and Surfaces*. CRC Press, Boca Raton, Florida, 1993.
3. L. H. KAUFFMAN. *On Knots*. Princeton Univ. Press, Princeton, New Jersey, 1987.
4. RAINDROP GEOMAGIC. <http://www.geomagic.com>.
5. D. ROLFSEN. *Knots and Links*. Publish or Perish, Houston, Texas, 1990.

## Appendix A

The formulas used to compute the cross-sections sweeping out torus knots are collected in this appendix. We write  $t = \omega \cdot s$ , where  $\omega$  is the number of times the spiral winds around the meridian. The location vector and its first three derivatives are

$$\begin{aligned} \Gamma(s) &= \begin{pmatrix} R \cos s - r \sin t \cos s \\ R \sin s - r \sin t \sin s \\ r \cos t \end{pmatrix}, \\ \dot{\Gamma}(s) &= \begin{pmatrix} -R \sin s + r \sin t \sin s - \omega r \cos t \cos s \\ R \cos s - r \sin t \cos s - \omega r \cos t \sin s \\ -\omega r \sin t \end{pmatrix}, \\ \ddot{\Gamma}(s) &= \begin{pmatrix} -R \cos s + 2\omega r \cos t \sin s + (\omega^2 + 1)r \sin t \cos s \\ -R \sin s - 2\omega r \cos t \cos s + (\omega^2 + 1)r \sin t \sin s \\ -\omega^2 r \cos t \end{pmatrix}, \\ \dddot{\Gamma}(s) &= \begin{pmatrix} R \sin s - (3\omega^2 + 1)r \sin t \sin s + (\omega^3 + 3\omega)r \cos t \cos s \\ -R \cos s + (3\omega^2 + 1)r \sin t \cos s + (\omega^3 + 3\omega)r \cos t \sin s \\ \omega^3 r \sin t \end{pmatrix}. \end{aligned}$$

Assuming  $0 < r < R$ , the second derivative vanishes if and only if  $\cos t = 0$  and  $R = (\omega^2 + 1)r \sin t$ . For many of the models in this paper we choose  $R = 2r$ , in which case  $\ddot{\Gamma}(s) = 0$  if and only if  $\omega = 1$  and  $s = 0$ .

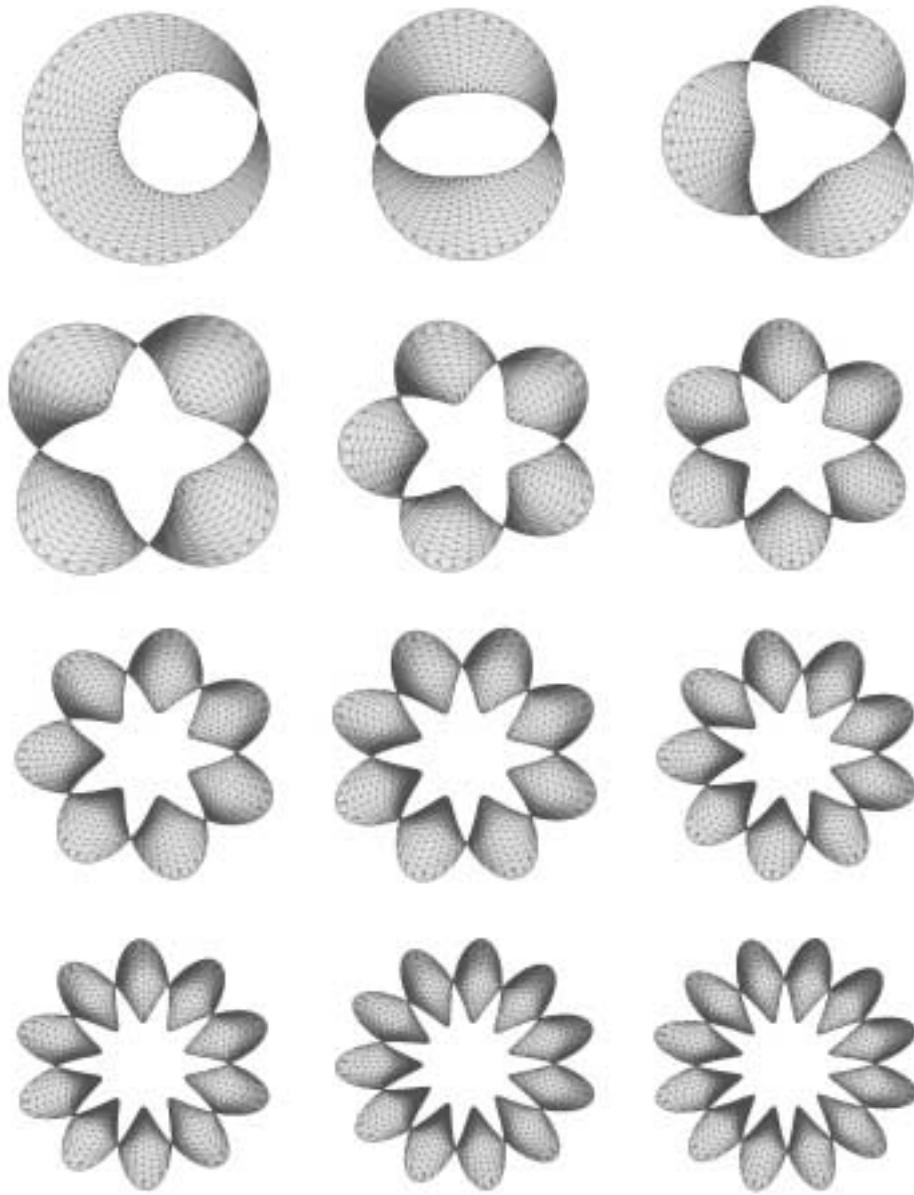


Figure 1: Line segment sweeping along circle in space. From left to right and top to bottom: the line segment rotates  $\frac{1}{2}, \frac{2}{2}, \frac{3}{2}$  times,  $\frac{4}{2}, \frac{5}{2}, \frac{6}{2}$  times,  $\frac{7}{2}, \frac{8}{2}, \frac{9}{2}$  times, and  $\frac{10}{2}, \frac{11}{2}, \frac{12}{2}$  times.

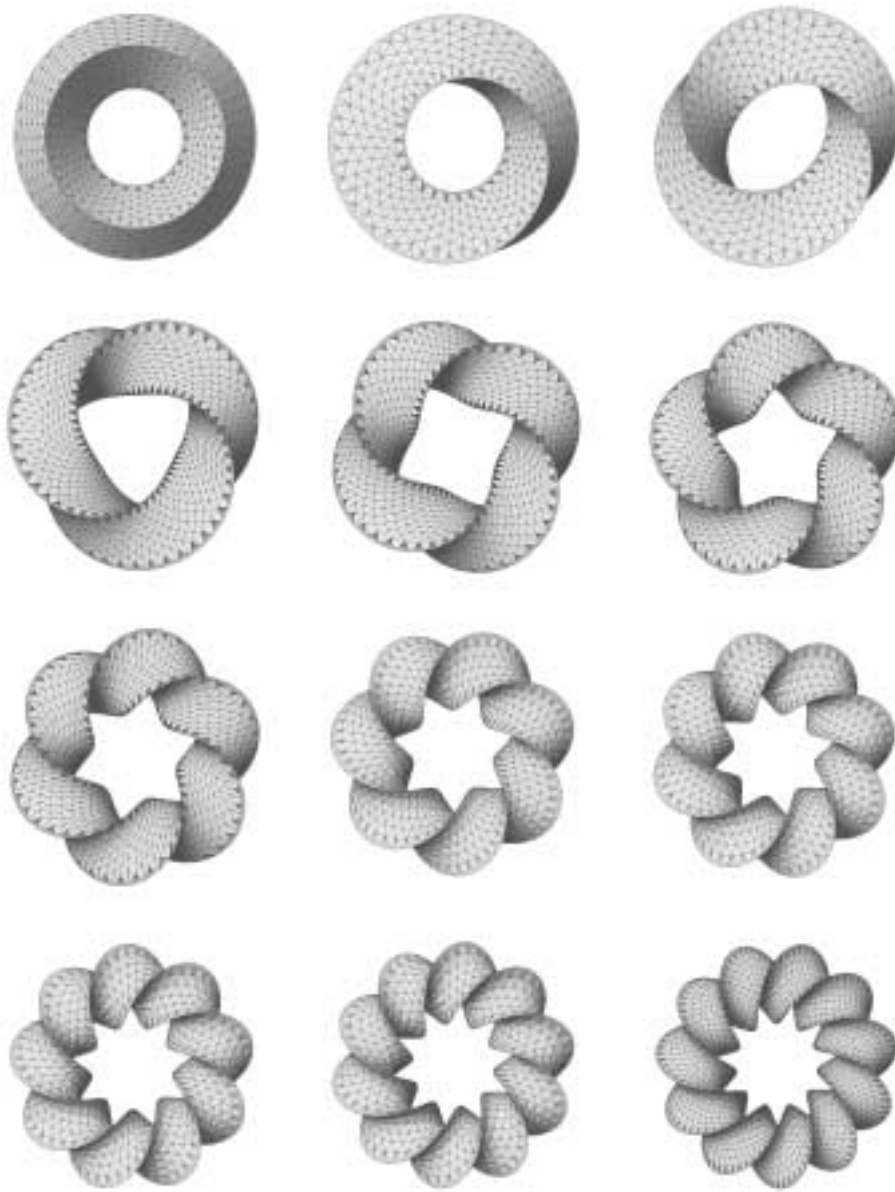


Figure 2: Triangle sweeping along circle in space. From left to right and top to bottom: the triangle rotates  $0, \frac{1}{3}, \frac{2}{3}$  times,  $\frac{3}{3}, \frac{4}{3}, \frac{5}{3}$  times,  $\frac{6}{3}, \frac{7}{3}, \frac{8}{3}$  times, and  $\frac{9}{3}, \frac{10}{3}, \frac{11}{3}$  times.



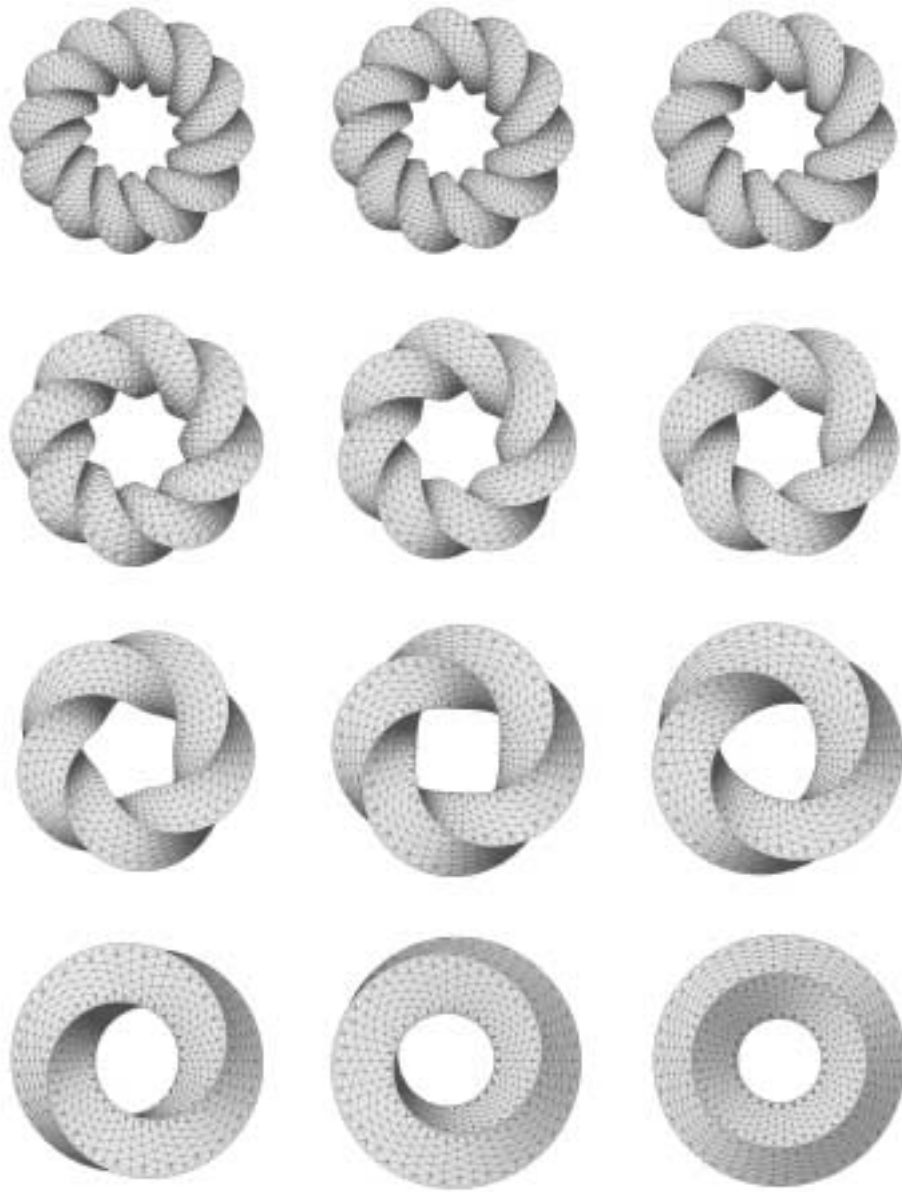


Figure 3: Square sweeping along circle in space. From left to right and top to bottom: the square rotates  $-\frac{12}{4}$ ,  $-\frac{11}{4}$ ,  $-\frac{10}{4}$  times,  $-\frac{8}{4}$ ,  $-\frac{7}{4}$ ,  $-\frac{6}{4}$  times,  $-\frac{5}{4}$ ,  $-\frac{4}{4}$ ,  $-\frac{3}{4}$  times, and  $-\frac{2}{4}$ ,  $-\frac{1}{4}$ , 0 times.

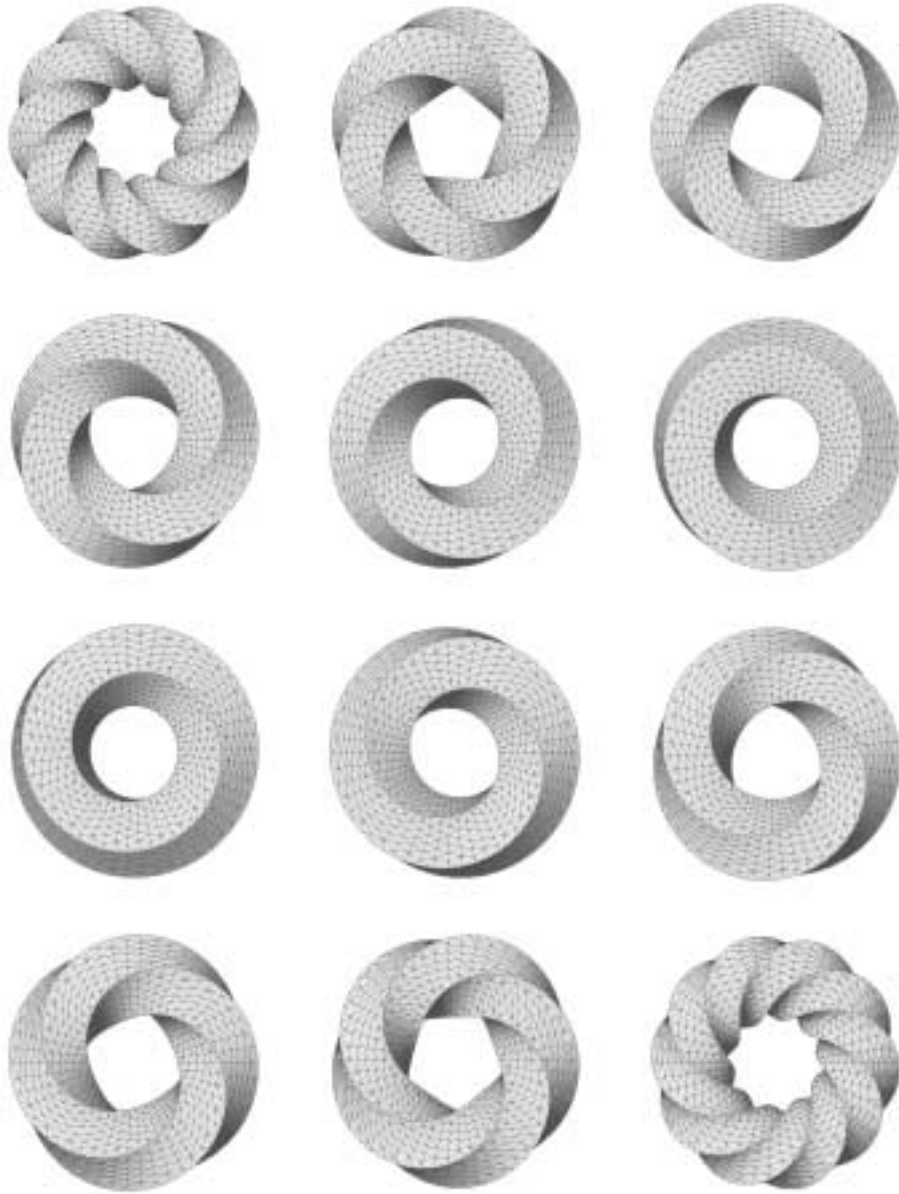


Figure 4: Pentagon sweeping along circle in space. From left to right and top to bottom: the pentagon rotates  $-\frac{10}{5}$ ,  $-\frac{5}{5}$ ,  $-\frac{4}{5}$  times,  $-\frac{3}{5}$ ,  $-\frac{2}{5}$ ,  $-\frac{1}{5}$  times,  $\frac{1}{5}$ ,  $\frac{2}{5}$ ,  $\frac{3}{5}$  times, and  $\frac{4}{5}$ ,  $\frac{5}{5}$ ,  $\frac{10}{5}$  times.

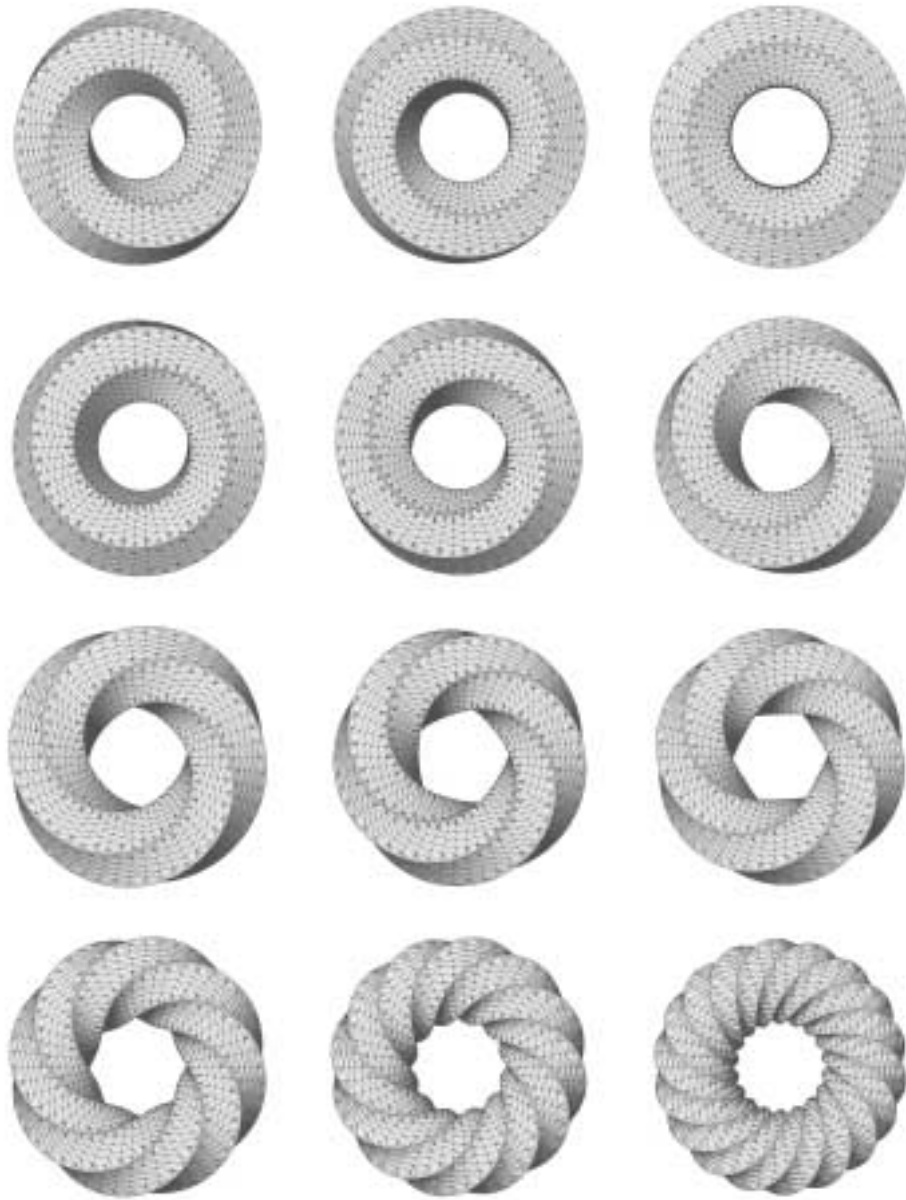


Figure 5: Hexagon sweeping along circle in space. From left to right and top to bottom: the hexagon rotates  $-\frac{2}{6}$ ,  $-\frac{1}{6}$ , 0 times,  $\frac{1}{6}$ ,  $\frac{2}{6}$ ,  $\frac{3}{6}$  times,  $\frac{4}{6}$ ,  $\frac{5}{6}$ ,  $\frac{6}{6}$  times, and  $\frac{8}{6}$ ,  $\frac{12}{6}$ ,  $\frac{18}{6}$  times.

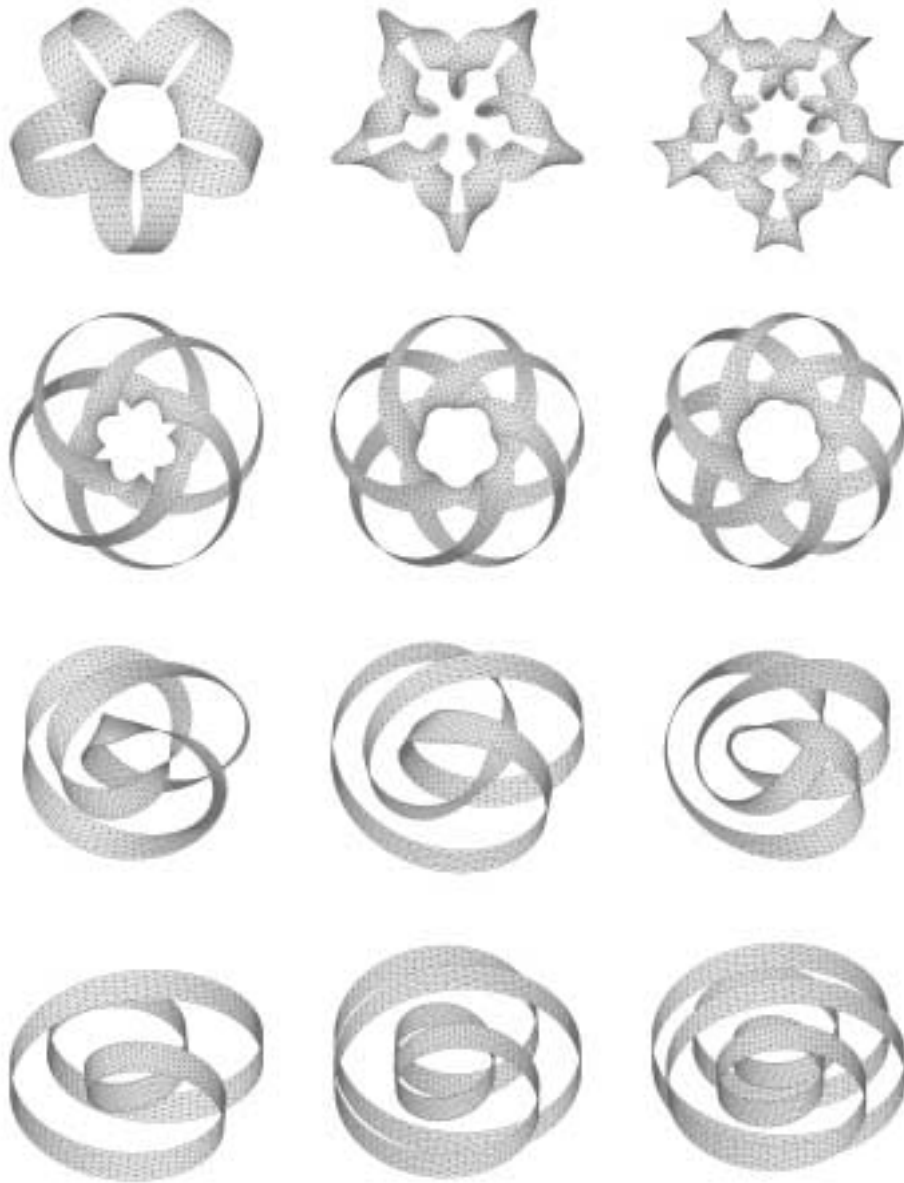


Figure 6: Line segment sweeping out flattened torus knots named  $(\lambda, \omega, \varrho)$ . From left to right and top to bottom:  $(1, 5, 0)$ ,  $(1, 5, \frac{10}{2})$ ,  $(1, 5, \frac{20}{2})$ , and  $(3, \frac{4}{3}, 0)$ ,  $(3, \frac{5}{3}, 0)$ ,  $(3, \frac{6}{3}, 0)$ , and  $(3, \frac{2}{3}, -\frac{2}{2})$ ,  $(3, \frac{2}{3}, 0)$ ,  $(3, \frac{2}{3}, \frac{2}{2})$ , and  $(3, \frac{1}{3}, 0)$ ,  $(4, \frac{1}{4}, 0)$ ,  $(5, \frac{1}{5}, 0)$ .

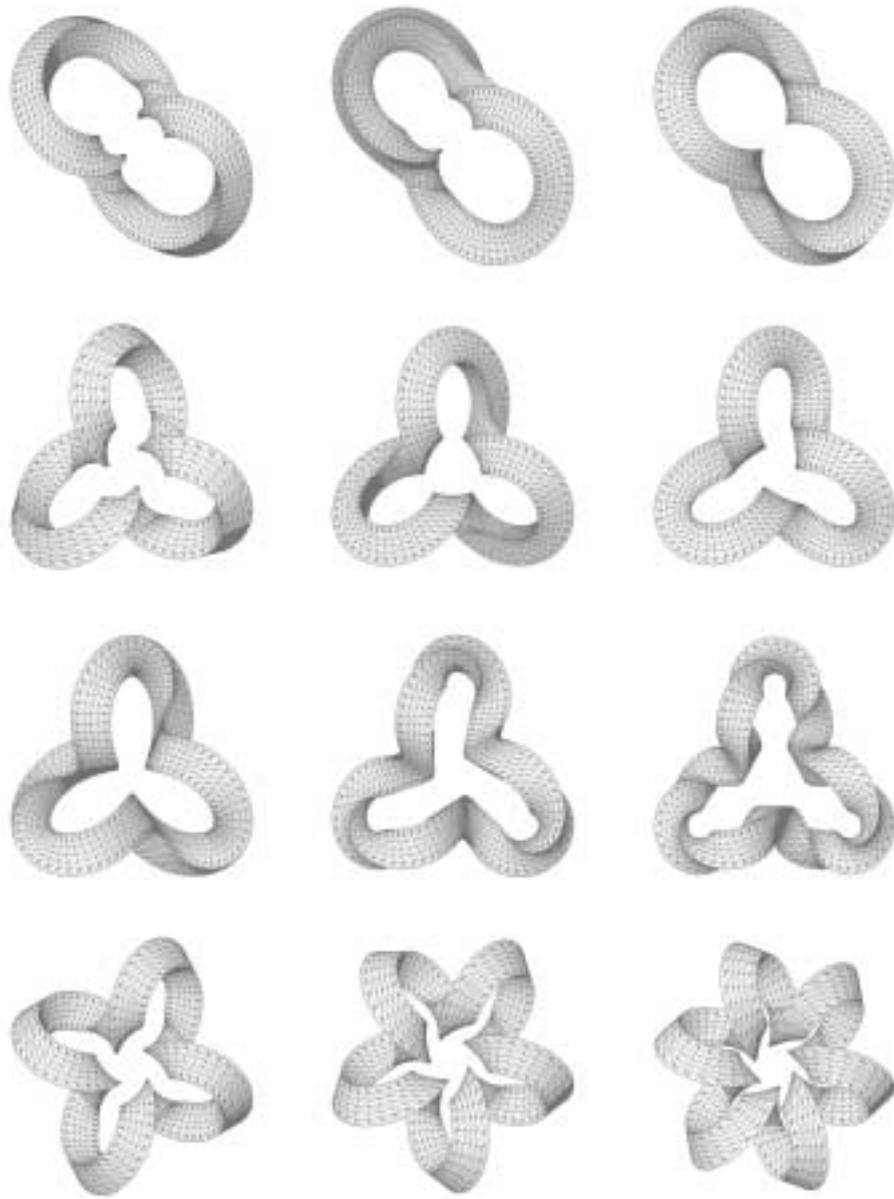


Figure 7: Triangle sweeping along torus knot. From left to right and top to bottom:  $(1, 2, 0)$ ,  $(1, 2, -\frac{3}{3})$ ,  $(1, 2, -\frac{6}{3})$ , and  $(1, 3, 0)$ ,  $(1, 3, -\frac{3}{3})$ ,  $(1, 3, -\frac{6}{3})$ , and  $(1, 3, -\frac{9}{3})$ ,  $(1, 3, -\frac{12}{3})$ ,  $(1, 3, -\frac{15}{3})$ , and  $(1, 4, 0)$ ,  $(1, 5, 0)$ ,  $(1, 6, 0)$ .

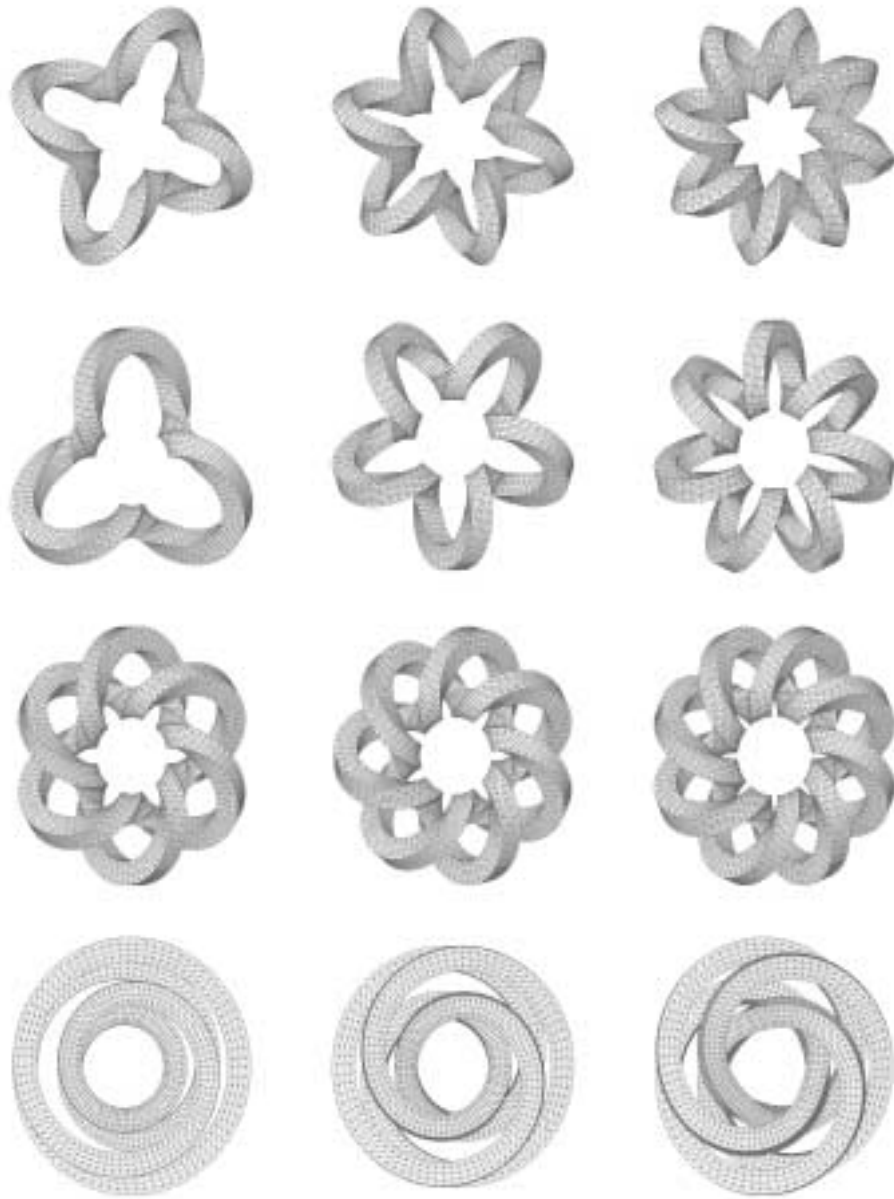


Figure 8: Square sweeping along torus knot. From left to right and top to bottom:  $(1, 4, 0)$ ,  $(1, 6, 0)$ ,  $(1, 8, 0)$ , and  $(1, 3, 0)$ ,  $(1, 5, 0)$ ,  $(1, 7, 0)$ , and  $(2, \frac{6}{2}, 0)$ ,  $(2, \frac{7}{2}, 0)$ ,  $(2, \frac{8}{2}, 0)$ , and  $(4, \frac{1}{4}, 0)$ ,  $(4, \frac{2}{4}, 0)$ ,  $(4, \frac{3}{4}, 0)$ .

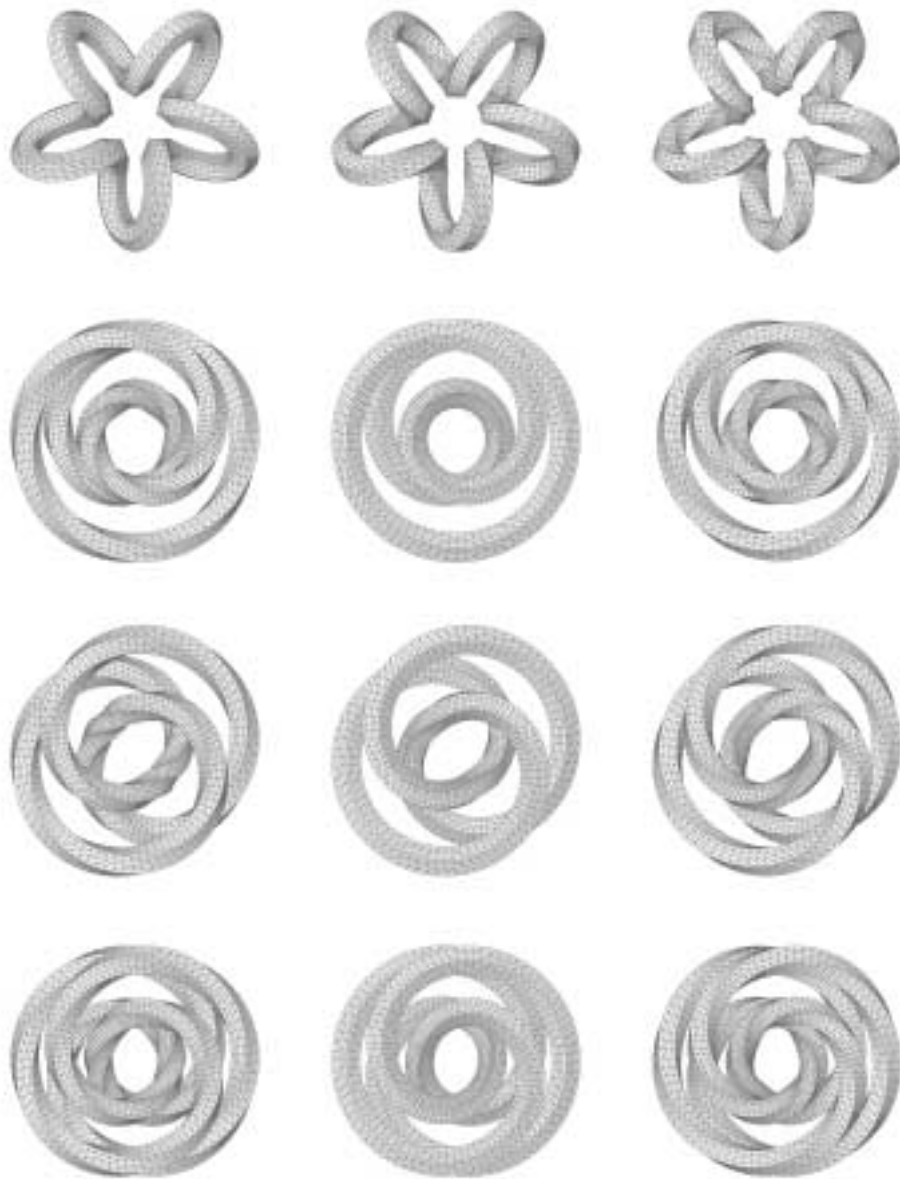


Figure 9: Pentagon sweeping along torus knot. From left to right and top to bottom:  $(1, 5, -\frac{10}{5})$ ,  $(1, 5, 0)$ ,  $(1, 5, \frac{10}{5})$ , and  $(3, -\frac{1}{3}, -\frac{5}{5})$ ,  $(3, -\frac{1}{3}, 0)$ ,  $(3, -\frac{1}{3}, \frac{5}{5})$ , and  $(3, \frac{2}{3}, -\frac{5}{5})$ ,  $(3, \frac{2}{3}, 0)$ ,  $(3, \frac{2}{3}, \frac{5}{5})$ , and  $(4, \frac{2}{4}, -\frac{5}{5})$ ,  $(4, \frac{2}{4}, 0)$ ,  $(4, \frac{2}{4}, \frac{5}{5})$ .

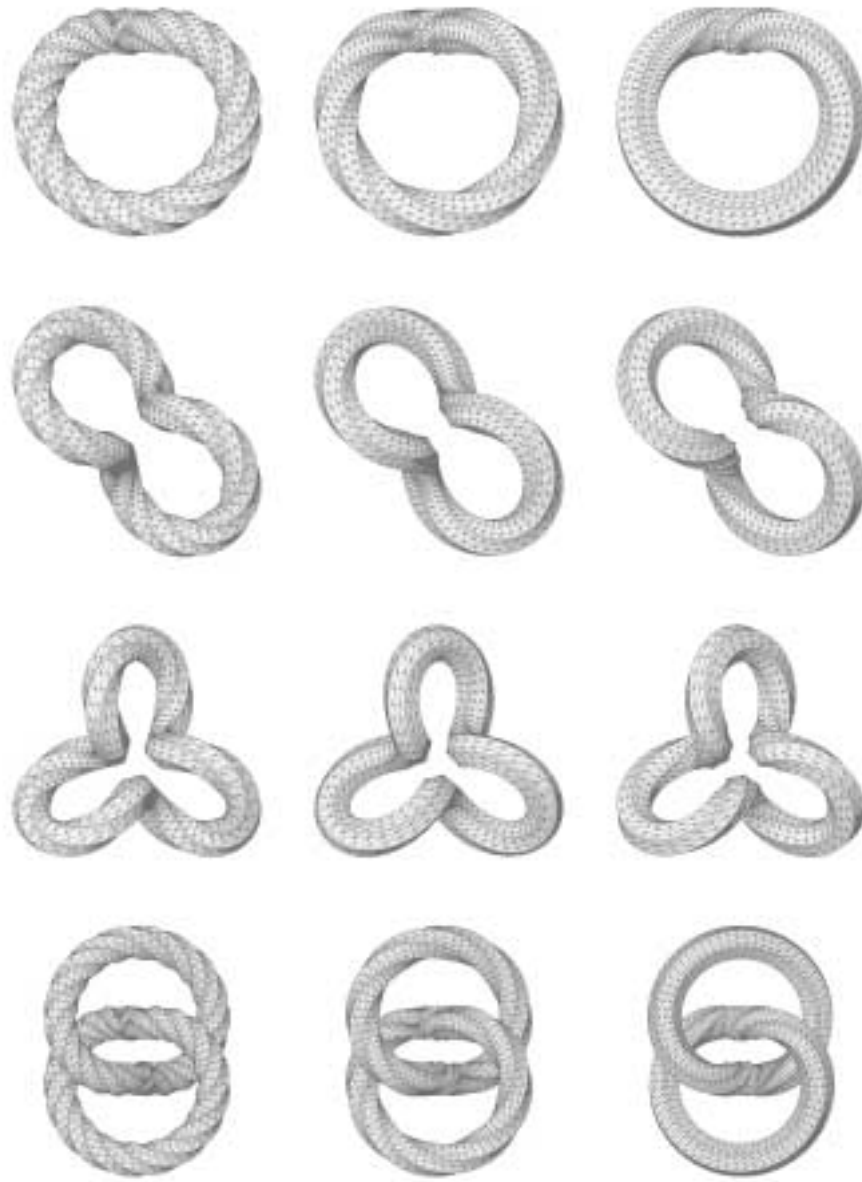


Figure 10: Hexagon sweeping along torus knot. From left to right and top to bottom:  $(1, 1, -\frac{24}{6})$ ,  $(1, 1, -\frac{12}{6})$ ,  $(1, 1, 0)$ , and  $(1, 2, -\frac{24}{6})$ ,  $(1, 2, -\frac{12}{6})$ ,  $(1, 2, 0)$ , and  $(1, 3, -\frac{24}{6})$ ,  $(1, 3, -\frac{12}{6})$ ,  $(1, 3, 0)$ , and  $(2, \frac{2}{2}, -\frac{24}{6})$ ,  $(2, \frac{2}{2}, -\frac{12}{6})$ ,  $(2, \frac{2}{2}, 0)$ .



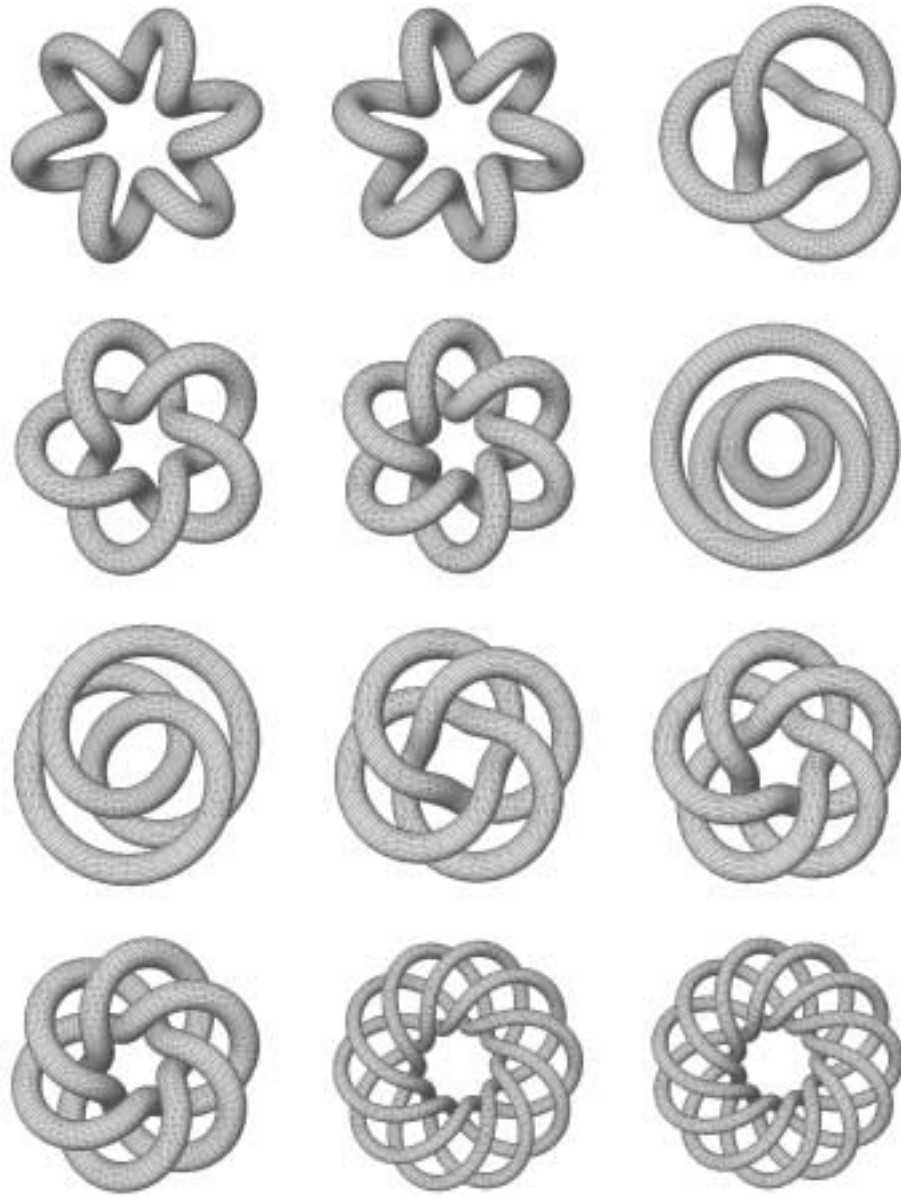


Figure 11: Circle sweeping out thickened torus knots named  $(\lambda, \omega)$ . From left to right and top to bottom:  $(1, -6)$ ,  $(1, 6)$ ,  $(2, \frac{3}{2})$ , and  $(2, \frac{5}{2})$ ,  $(2, \frac{6}{2})$ ,  $(3, \frac{1}{3})$ , and  $(3, \frac{2}{3})$ ,  $(3, \frac{4}{3})$ ,  $(3, \frac{5}{3})$ , and  $(3, \frac{6}{3})$ ,  $(4, \frac{10}{4})$ ,  $(4, \frac{11}{4})$ .

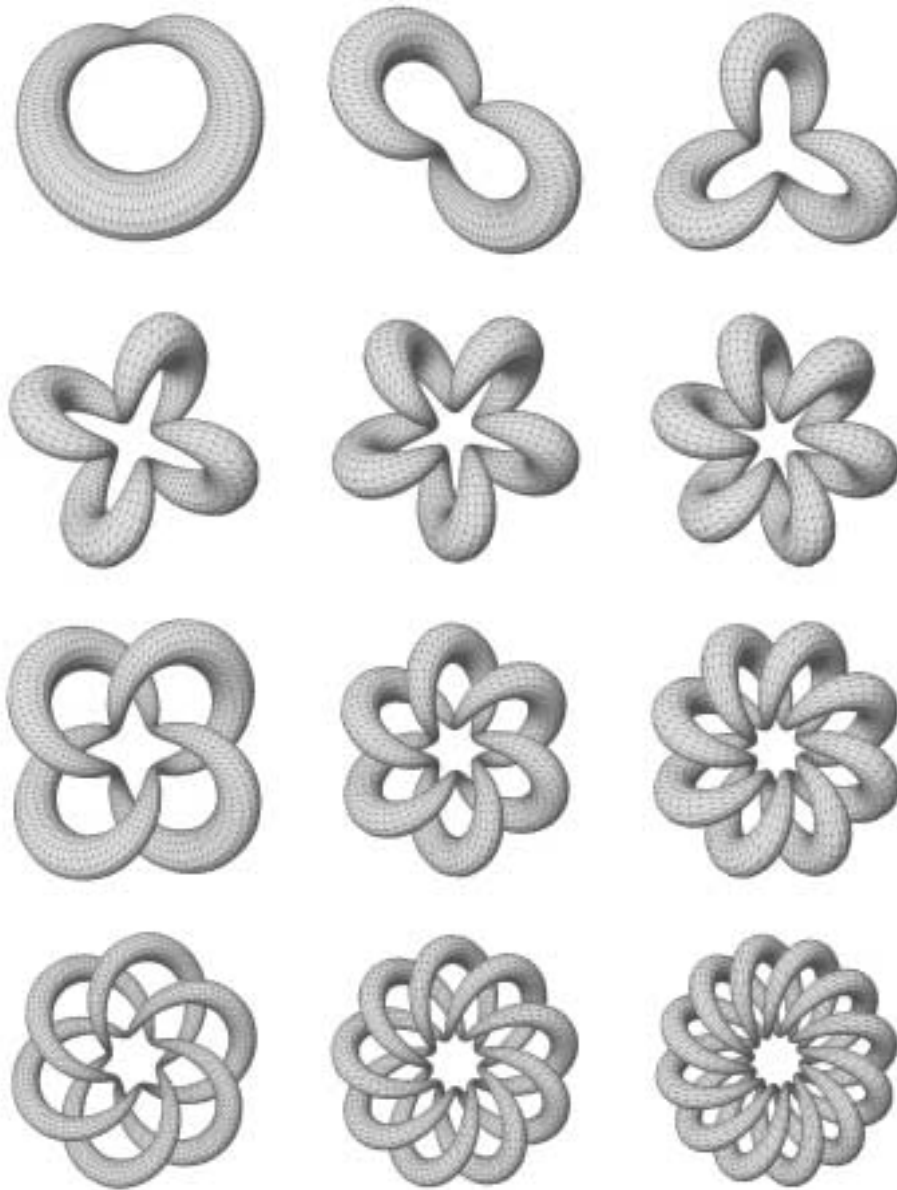


Figure 12: The cross-section is a circle that grows proportional to the norm. From left to right and top to bottom:  $(1, 1)$ ,  $(1, 2)$ ,  $(1, 3)$ , and  $(1, 4)$ ,  $(1, 5)$ ,  $(1, 6)$ , and  $(2, \frac{4}{2})$ ,  $(2, \frac{6}{2})$ ,  $(2, \frac{8}{2})$ , and  $(3, \frac{6}{3})$ ,  $(3, \frac{9}{3})$ ,  $(3, \frac{12}{3})$ .

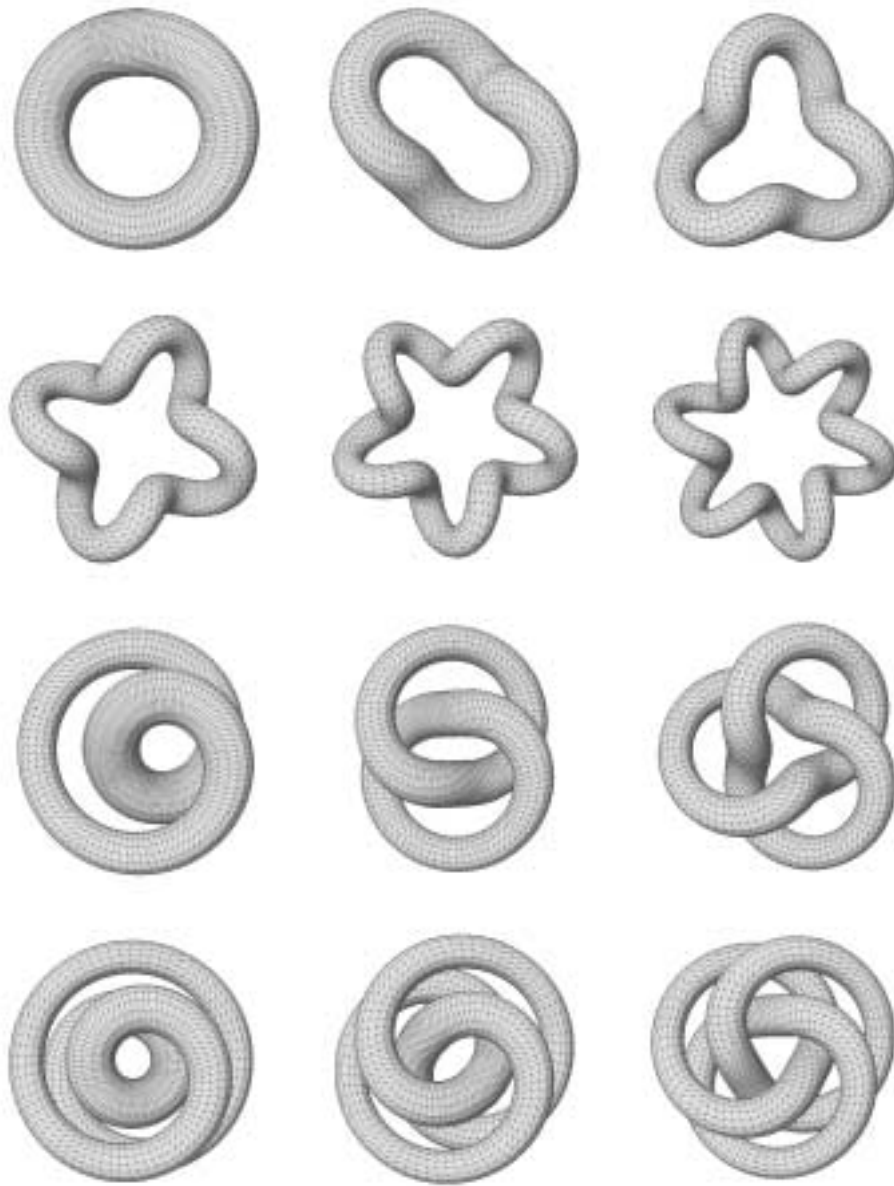


Figure 13: The cross-section is a circle that shrinks with increasing speed. From left to right and top to bottom:  $(1, 1)$ ,  $(1, 2)$ ,  $(1, 3)$ , and  $(1, 4)$ ,  $(1, 5)$ ,  $(1, 6)$ , and  $(2, \frac{1}{2})$ ,  $(2, \frac{2}{2})$ ,  $(2, \frac{3}{2})$ , and  $(3, \frac{1}{3})$ ,  $(3, \frac{2}{3})$ ,  $(3, \frac{3}{3})$ .

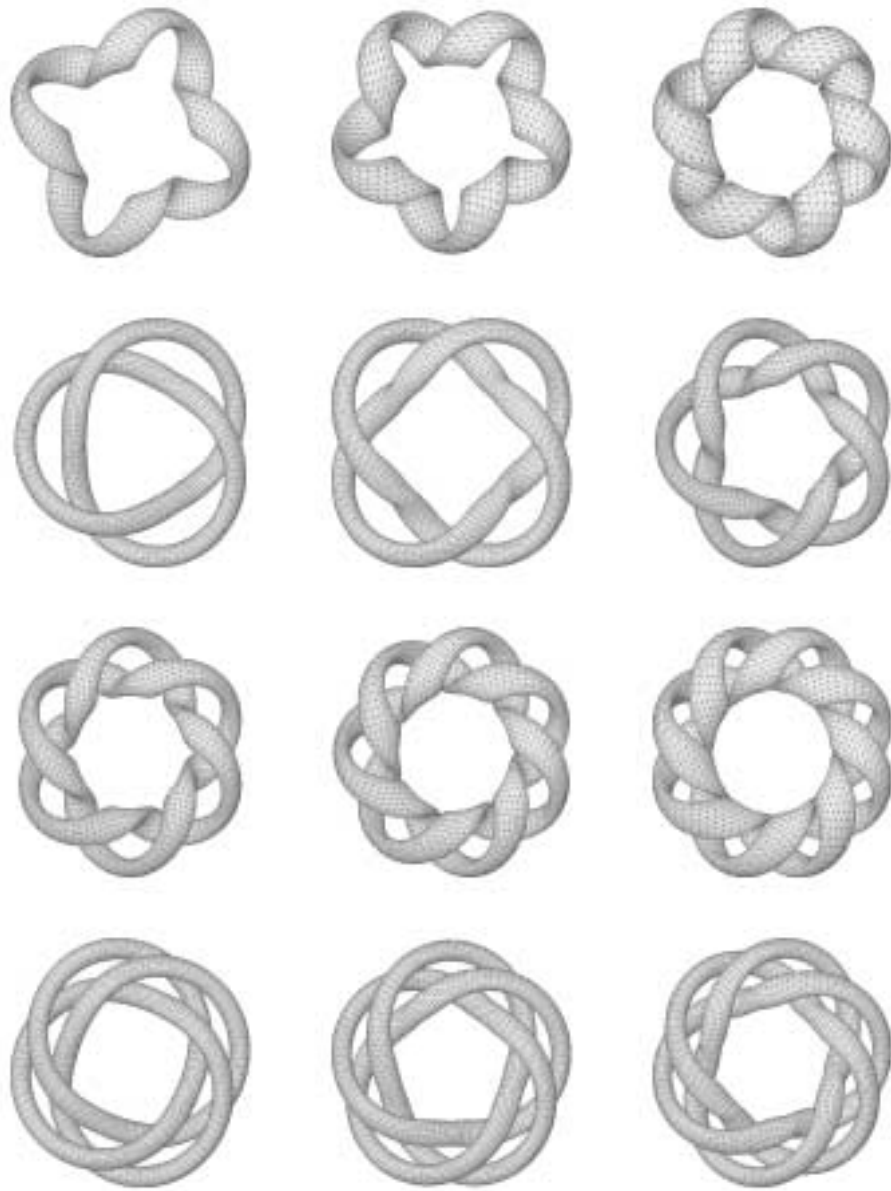


Figure 14: The cross-section is an ellipse that grows wider and flatter as the curvature increases. From left to right and top to bottom:  $(1, 4)$ ,  $(1, 5)$ ,  $(1, 6)$ , and  $(2, \frac{3}{2})$ ,  $(2, \frac{4}{2})$ ,  $(2, \frac{5}{2})$ , and  $(2, \frac{6}{2})$ ,  $(2, \frac{7}{2})$ ,  $(2, \frac{8}{2})$ , and  $(3, \frac{4}{3})$ ,  $(3, \frac{5}{3})$ ,  $(3, \frac{6}{3})$ .

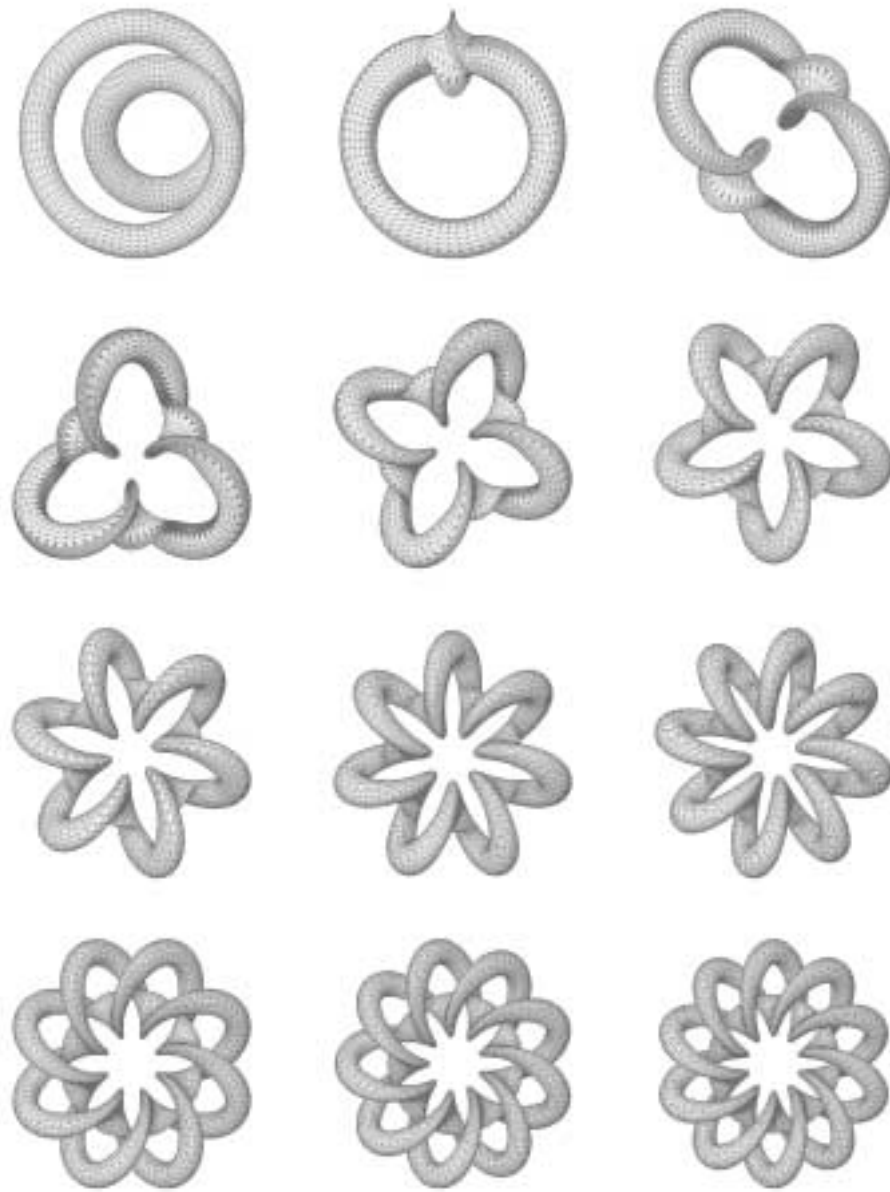


Figure 15: The cross-section is an ellipse that grows narrower and taller with increasing torsion. From left to right and top to bottom:  $(2, \frac{1}{2})$ ,  $(1, 1)$ ,  $(1, 2)$ , and  $(1, 3)$ ,  $(1, 4)$ ,  $(1, 5)$ , and  $(1, 6)$ ,  $(1, 7)$ ,  $(1, 8)$ , and  $(2, \frac{8}{2})$ ,  $(2, \frac{9}{2})$ ,  $(2, \frac{10}{2})$ .